

## Supporting Information

### Non-conjugated Diketone as Linkage for Enhancing the Rate Performance of Poly(perylenediimides)

Xiang Gao,<sup>1, #</sup> Yuan Chen,<sup>2, #</sup> Chengjun Gu,<sup>1, #</sup> Jing Wen,<sup>1,3,\*</sup> Xiang Peng,<sup>1</sup> Jiacheng Liu,<sup>1</sup> Zhanhui Zhang,<sup>1</sup> Zhitian Liu,<sup>1,\*</sup> and Chengliang Wang<sup>2,\*</sup>

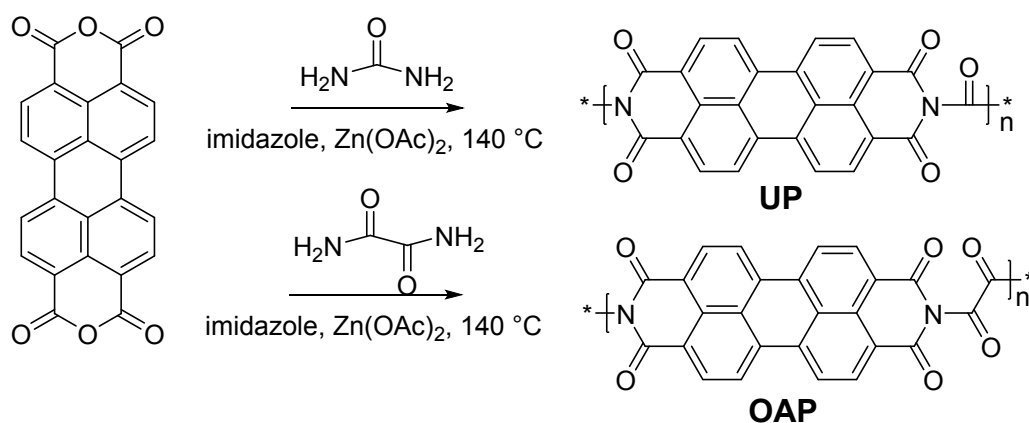
<sup>1</sup> Hubei Engineering Technology Research Center for Optoelectronic and New Energy Materials, School of Materials Science and Engineering, Wuhan Institute of Technology, Wuhan 430205, P. R. China

<sup>2</sup> School of Optical and Electronic Information, Wuhan National Laboratory for Optoelectronics (WNLO), Huazhong University of Science and Technology, Wuhan 430074, China

<sup>3</sup> School of Chemistry and Chemical Engineering, Nanjing University, Nanjing 210023, P. R. China

# these authors contributed equally.

### Materials synthesis



**Scheme 1.** Synthetic scheme for the poly(PDI)s: UP and OAP.

Synthesis of **UP** and **OAP**: 2 mmol of 3,4,9,10-perylenetetracarboxylic dianhydride (PTCDA) was mixed with 2 mmol of diamine (urea or oxamide), 2 mmol of zinc acetate and 7.8 g of imidazole in a flask, then the mixture was heated to 140 °C with stirring for 24 h. When the reaction was finished, the mixture was cooled to 90 °C, and hydrochloric acid with

a concentration of 1 mol L<sup>-1</sup> was added. After stirring for another 20 min, the solution was filtrated and the precipitate was washed with saturated potassium carbonate solution, then distilled water three times. The precipitate was further washed with DMSO until the washings became almost colorless. The precipitate was finally washed with distilled water for three times to remove possible residual DMSO and dried in air at 110 °C for 12 h. The solid state <sup>13</sup>C NMR was performed on a JEOL 500 MHz NMR spectrometer.

1. Urea-erylene diimide polymer (UP): The polymer was synthesised with PTCDA and urea. Dark purple powder was obtained with a yeild of 64.6 %. Solid state <sup>13</sup>C NMR (150 MHz δ): 166.42 (C=O), 162.65 (C=O), 133.07 (Ar-C), 124.05 (Ar-C). The element analysis of as-synthesised polymer: N 6.07%, C 71.69%, H 2.53%, O 19.71%.

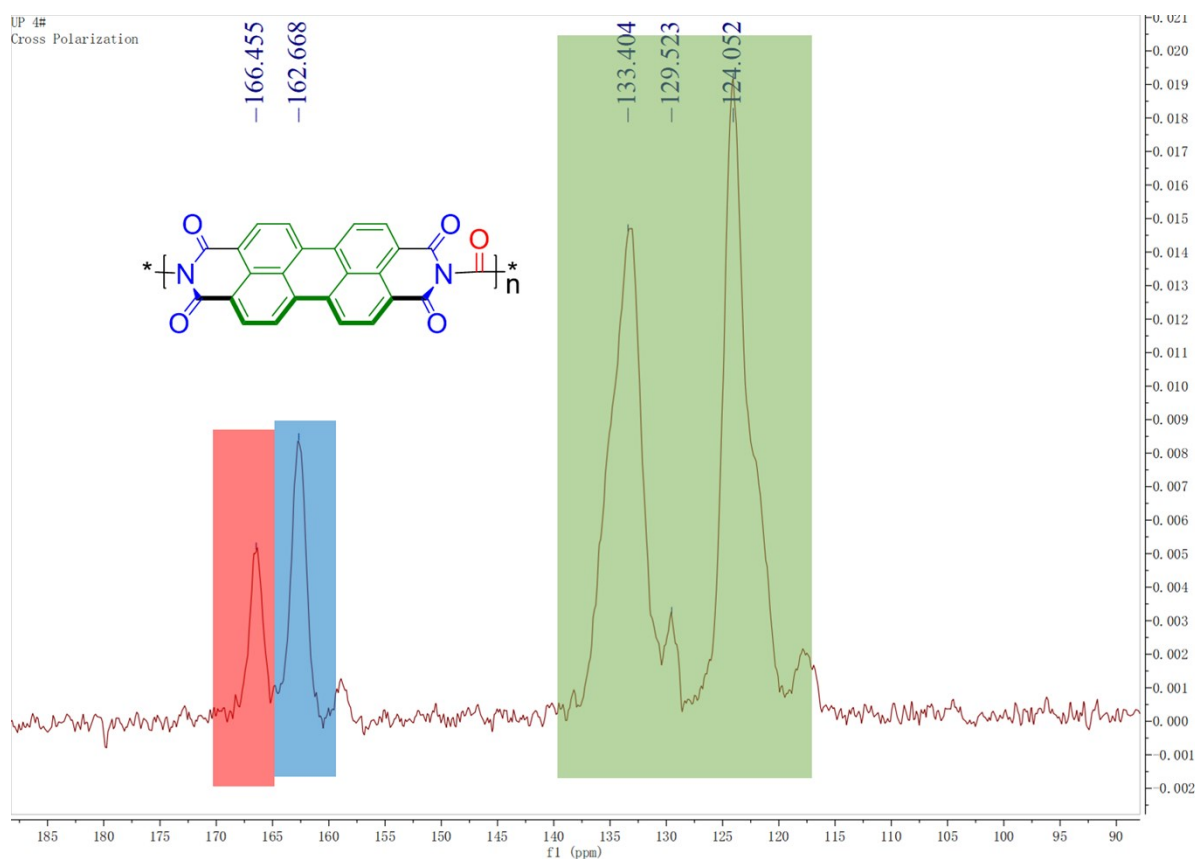


**Figure S1.** Solid state <sup>13</sup>C NMR spectrum of UP.

2. Oxamide-erylene diimide polymer (OAP): The polymer was synthesised with PTCDAs and oxamide. Dark purple powder was obtained with a yeild of 70.7 %. Solid state  $^{13}\text{C}$  NMR (150 MHz  $\delta$ ): 166.59 (C=O), 162.84 (C=O), 133.28 (Ar-C), 124.17 (Ar-C). The element analysis of as-synthesised polymer: N 5.65 %, C 71.14 %, H 2.72 %, O 20.49 %.

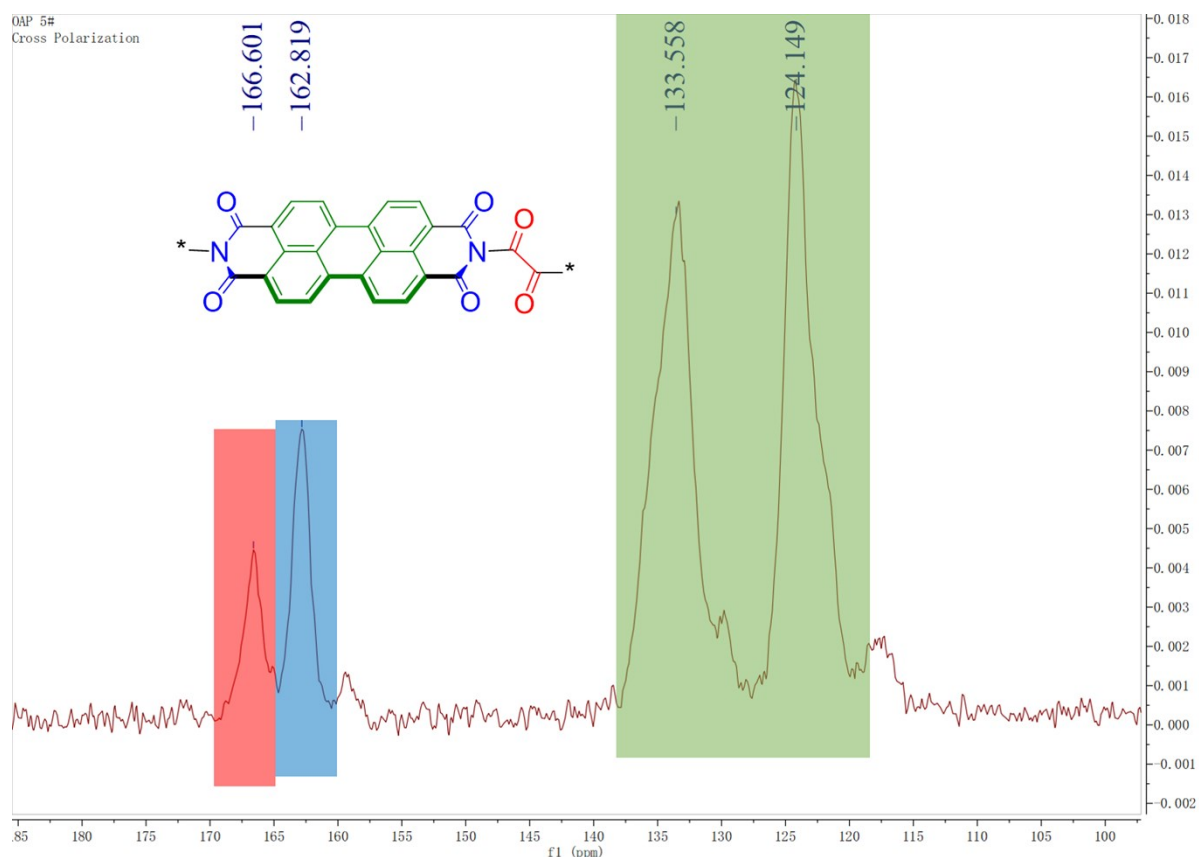


**Figure S2.** Solid state  $^{13}\text{C}$  NMR spectrum of OAP.

### Cell fabrication and characterization

To evaluate the electrochemical performance, the electrodes were prepared by mixing the active material with super P and polyvinylidene fluoride (PVDF) in a weight ratio of 5:4:1, using N-methyl-2-pyrrolidone (NMP) as solvent. Then the slurry was coated on Al foil and dried overnight in vacuum at 80 °C. The 2032 coin-type cells were assembled in Ar-filled glove box with water and oxygen level under 1.0 ppm. The sodium was used as the counter electrode. Glass fiber membrane (Whatman, GF/B) was used as separator and 1 M  $\text{NaPF}_6$

dissolved in dimethyl ether (DME) was used as electrolyte. The mass loading of active material is about 0.9~1.3 mg, 1.6~2.0 mg or 2.6~3.2 mg (for optimizing the mass lading) at each electrode disc (area: 1.54 cm<sup>2</sup>). Galvanostatic experiments were performed at a different current densities at a potential range of 3.5–1.0 V (versus Na/Na<sup>+</sup>) with a LANHE-CT2001A test system (Wuhan, China) at room temperature. CV and EIS were performed on a BioLogic VSP potentiostat. The CV curves were scanned in the potential range from 3.5 to 1.0 V at the scan rates of 0.5 mV s<sup>-1</sup>. For EIS tests, the voltage amplitude was 10 mV and the frequency range was 1.0 MHz to 5 mHz. For ex situ FT-IR, XRD and SEM characterizations, coin cells were cycled to a certain state of charge and disassembled in an Ar-filled glovebox. Sodium carboxymethylcellulose was used as binder for XRD measurements and PVDF was used for other experiments. The electrodes were washed by DME and dried in vacuum.

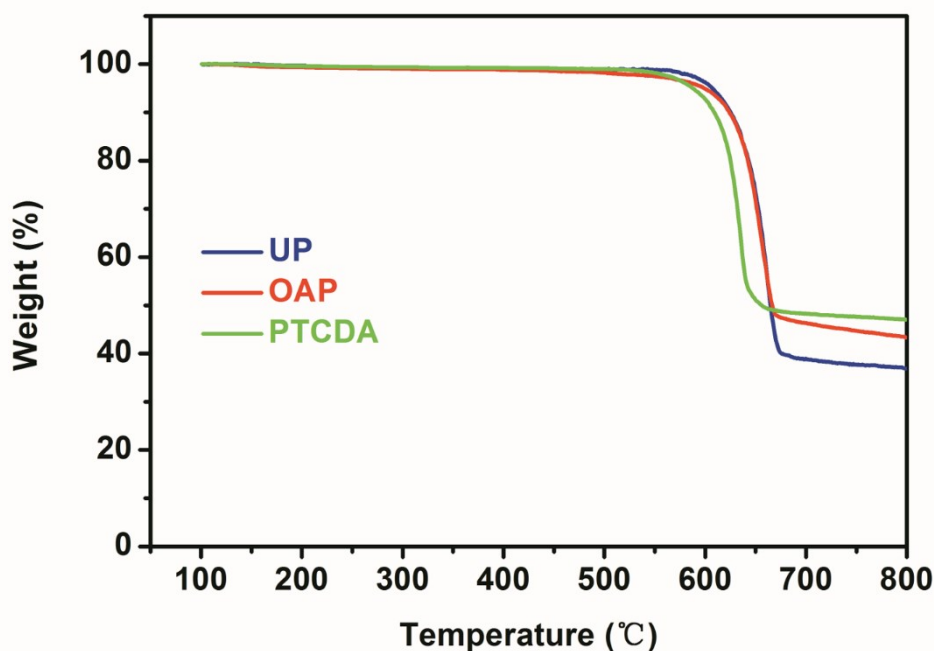


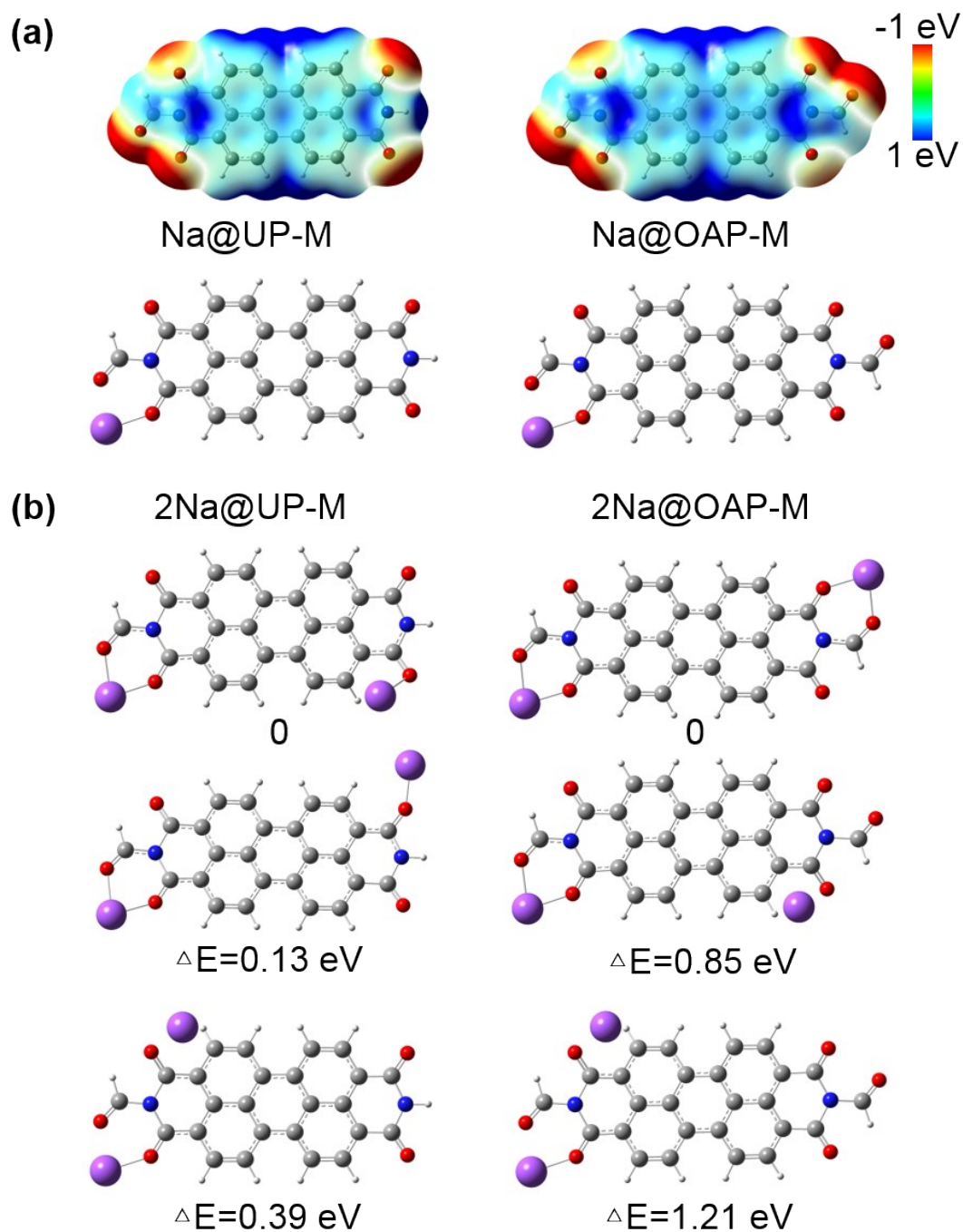
**Figure S3.** TGA curves of PTCDA, UP and OAP.

## Computational method

The UP and OAP monomers are hydrogen-capped repeat units, and their dimers are two repeat units end-capped with half PDI. These selected models are, on the one hand, beneficial to clearly illustrate the function of the linkage carbonyl by investigating monomers without neighbors, and on the other hand, more approximate to the experimental adsorption of sodium cation by investigating dimers capped with half PDI. All the calculations of geometry optimizations and molecular orbitals were performed with Gaussian 09, Revision D.0.1.<sup>S1</sup> The density functional theory (DFT) was applied at the level of B3LYP/6-311++g(d) for compromise of calculation cost and accuracy. From theoretical calculations, the electrochemical inactive property of linkage carbonyl in UP and OAP can be showed directly via the molecular orbital distributions, and the adsorption energy per sodium ( $E_a$  is calculated with equation S1) is somehow related to the rate performance.

$$E_a = (E_{\text{Na@model}} - nE_{\text{Na}} - E_{\text{model}}) / n \quad (\text{S1})$$

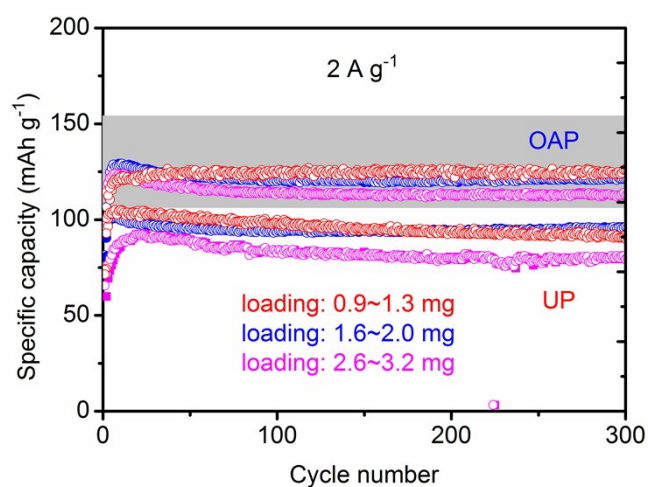
Where  $E_{\text{Na@model}}$  is the total energy of the whole optimized sodium-adsorbed model,  $n$  is the number of sodium atoms, and  $E_{\text{model}}$  is the current energy of the remaining part of sodium-adsorbed model without sodium atoms. Therefore, more negative value of  $E_a$  means stronger adsorption of sodium atoms.



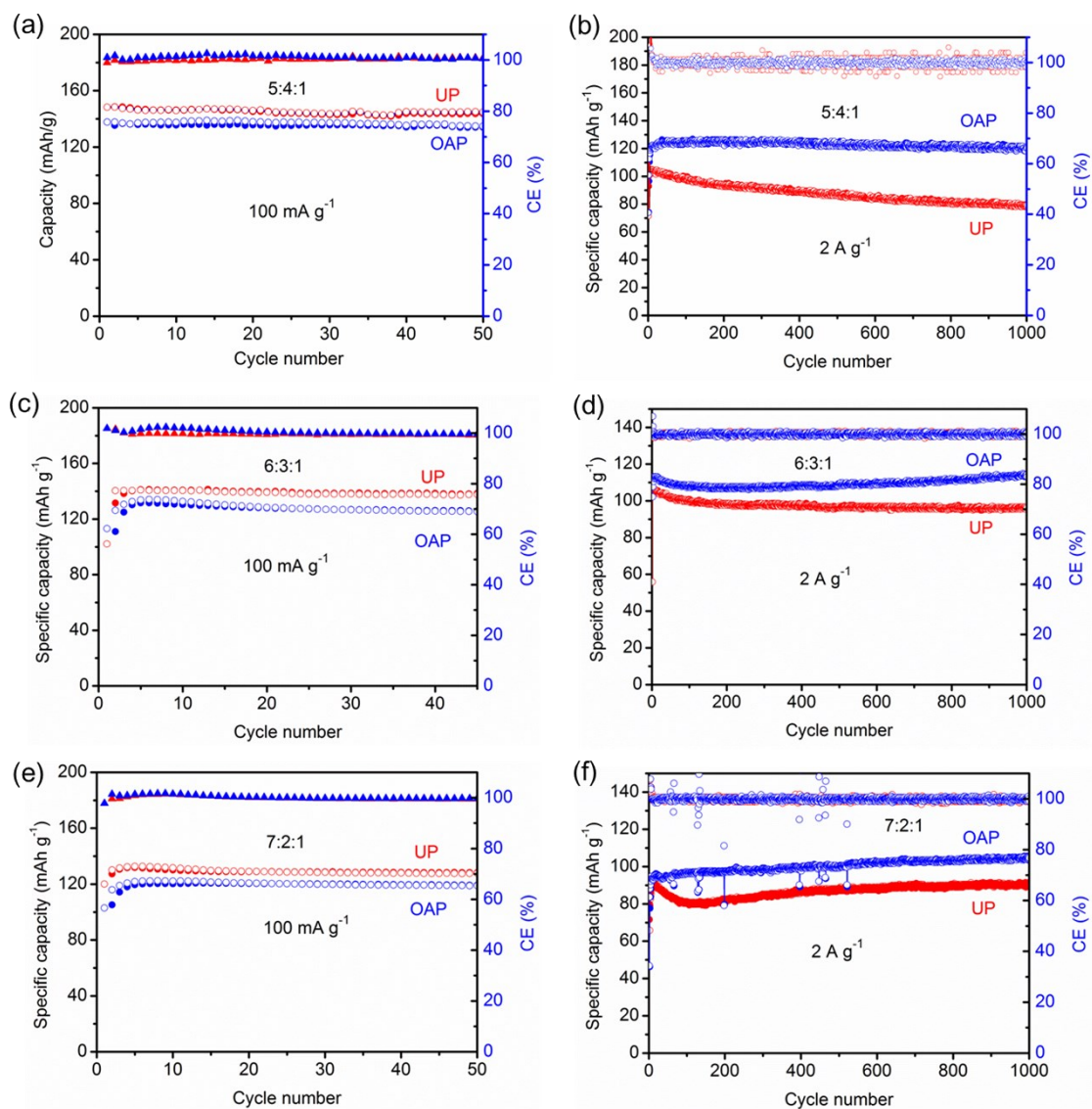
**Figure S4.** The adsorption structures of UP and OAP monomer with one or two sodium cations. The first sodium cation adsorption structure can be easily figured out from the electrostatic potential distribution (a). The second sodium cation has three most possible adsorption sites (b). The most stable structure is marked with relative energy ( $\Delta E$ ) of 0 below, and the higher energy structures are showed with the positive  $\Delta E$ , namely the total energy difference of the current structure with the most stable structure.

**Table S1.** Measured and calculated elements

	N%		O%		$\bar{DP}$	Molecular weight
	Measured	Calculated	Measured	Calculated		
OAP	5.65	5.6	20.49	21.93	7	3502.7
UP	6.07	6.15	19.71	19.67	10	4555.6



**Figure S5.** Comparison of high rate cycling in different mass loading of active materials. As shown in Figure S5, the high rate cycling of the two materials did not change significantly within a certain load range (0.9 mg~2.0 mg at each electrode disc). When the mass loading of active materials further increased to about 3.2 mg, the performance decreased. Particularly, the electrochemical performance of UP decreased more significantly than that of OAP, further proving that non-conjugated diketone can contribute to the coordination with Na<sup>+</sup> and the rate performance.

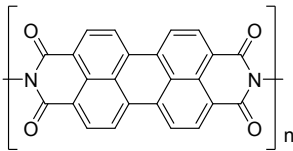
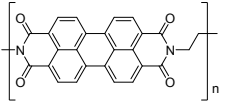
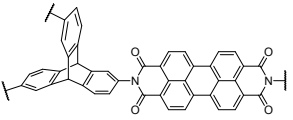
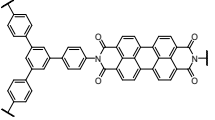
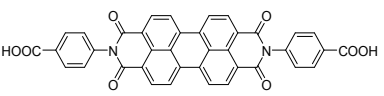
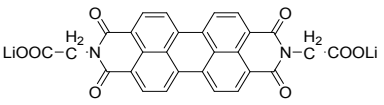
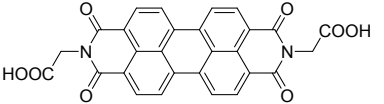


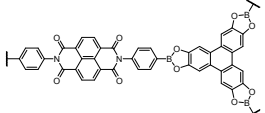
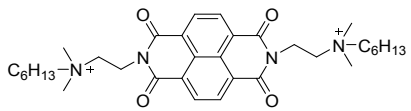
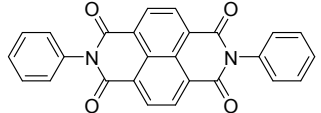
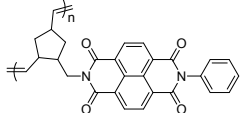
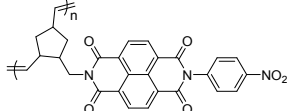
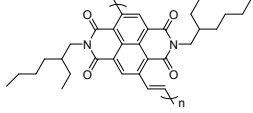
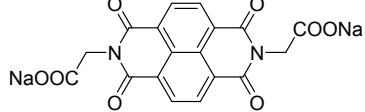
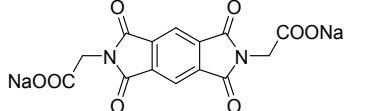
**Figure S6.** Comparisons of the cycle stability of UP and OAP at 100 and 2000  $\text{mA g}^{-1}$ , respectively, with different ratios of active materials. As shown in Figure S6, higher content of electrode materials will result in an activation process in the first several cycles and a significant reduction in capacity at high rate. Compared with UP, OAP also showed better electrochemical performance at high rate even at high proportion of electrode materials. What's more, it should be noted that even at high content of active materials, the comparison between the two active materials showed the similar phenomena: OAP showed slightly lower capacity at slow rate (because of its lower theoretical capacity), but much higher actual

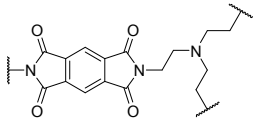
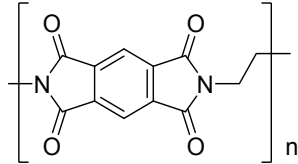
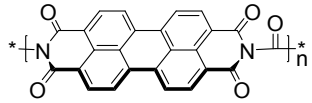
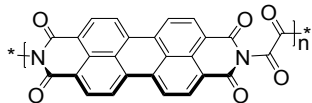


capacity at high rate, indicating that the non-conjugated diketone can contribute to the coordination with  $\text{Na}^+$  and the rate performance.

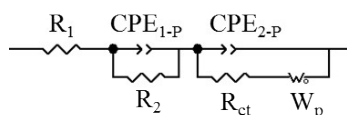
**Table S2.** The cycling performances of diimide-based electrodes at different current densities published in recent five years.

	Cycles	Current density mA g <sup>-1</sup>	Initial capacity mA h g <sup>-1</sup>	Final capacity mA h g <sup>-1</sup>	Ref.	Metal ion
	50	50	126	101	10.1039/C5TA 02043C	Na
	50	800	106	62		
	50	50	130	110	10.1021/jz401 7359	Li
	50	50	85	75	10.1021/jz401 7359	Li
	500	152	76	61	10.1021/acsam i.7b02336	Li
	65	25	78.1	58	10.1039/c3ra4 5563g	Li
	200	425	95	71	10.1021/cm50 46786	Li
	200	850	114	80		
	200	1550	68	55		
	1000	200	94	87	10.1016/j.elect acta.2017.02.1 52	Li
	200	2000	78	70	10.1002/slct.20 1801588	Li

	700	200	74	74	10.1038/srep08225	Li
	260	25	177	170	10.1039/c5ra26181c	Li
	100	25	182	121	10.1038/srep23515	Li
	500	112	119	119	10.1557/mrc.2017.127	Li
	500	103	87	87		
	100	20.2	110	50	10.1149/2.1011702jes	Li
	60	50	121	94	10.1149/2.0221701jes	Na
	100	100	110	87		
	100	150	100	86		
	50	50	135	36	10.1149/2.0221701jes	Na
	50	100	97	32		
	50	150	79	36		

	200	192	147	128	10.1002/adma. 201502241	Li
	200	222	147	147	10.1002/adma. 201305452	Li
	180	50	200	210	10.1039/C6TA 09754E	Na
	1000	1000	116	85		
	500	140	142	126	10.1039/c4ra0 3473b	Na
	500	100	148.3	141.5	This work	Na
	1000	2000	105.1	78.9		
	500	100	137.8	127.4		
	1000	2000	124.8	120.9		

**Table S3.** The equivalent circuit and the values of the electrical elements of the electrodes.



Samples	$R_1$	Error (%)	$R_2$	Error (%)	$CPE_{1-P}$	Error (%)	$R_{ct}$	Error (%)	$CPE_{2-P}$	Error (%)	$W_p$	Error (%)	
UP	1	2.11	0.02	26.7	1.5	0.832	0.0047	15.8	1.63	0.71	0.03	0.62	0.002
	5	2.2	0.77	34.9	1.55	0.85	1.33	47.9	1.59	0.78	0.29	0.59	0.46
	10	1.5	0.91	20.79	2.07	0.896	1.03	52	1.55	0.82	0.2	0.31	2.01
	20	2.53	1.77	30	8.3	0.92	0.72	62	5.11	0.8	5.02	0.36	2.09
OAP	1	2.5	0.93	6.8	0.24	1.002	1.54	26.1	0.32	0.93	0.001	0.42	0.002
	5	1.3	1.2	19.8	1.43	0.88	1.4	27.1	1.25	0.83	0.16	0.43	0.55
	10	1.33	1.48	20.1	1.57	0.9	1.36	25.4	1.61	0.81	0.26	0.42	1.23
	20	1.72	1.87	20.3	9.2	0.93	0.65	21	9.4	0.82	3.6	0.4	1.8

The equivalent circuit was inserted in Table S3, where  $R_1$ ,  $R_2$ , CPE,  $R_{ct}$ , and  $W_p$  represent the electrolyte resistance, interfacial resistance, constant phase element, charge-transfer resistance and Warburg resistance, respectively.  $CPE_{1-P}$  and  $CPE_{2-P}$  are related to the capacitive behavior of the interface and electrodes, respectively.

**Table S4.** The calculated Warburg impedance coefficient ( $\sigma_w$ ) of UP and OAP after 1 and 10 cycles.

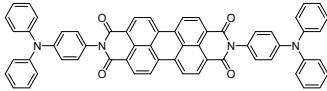
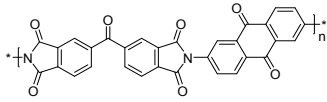
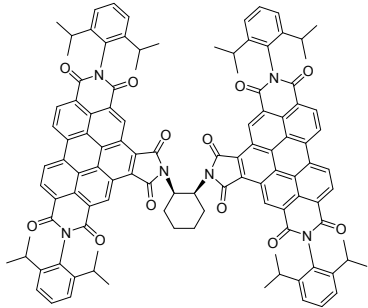
	$\sigma_w$	
	1st cycle	10th cycle
UP	7.9	6.6
OAP	6.5	2.0

**Table S5.** Na-ion diffusion coefficient of representative electrodes in SIBs

Materials	Technique	Diffusion coefficient (cm <sup>2</sup> s <sup>-1</sup> )	Ref.
UP	EIS	$2.6 \times 10^{-12}$	This work
AP	EIS	$2.9 \times 10^{-11}$	
Na <sub>2</sub> C <sub>6</sub> O <sub>6</sub>	EIS	$7.9 \times 10^{-16}$	10.1021/acs.nanolett.6b00954
PPTS	CV	$2.2 \times 10^{-9}$	
P-SPAN	GITT	$\sim 1.0 \times 10^{-9}$	10.1016/j.chempr.2018.08.014
P/SPAN	GITT	$1.0 \sim 2.3 \times 10^{-11}$ $1 \sim 9 \times 10^{-12}$	10.1002/adfm.201801010
KTL	CV	$1.1 \sim 2.26 \times 10^{-9}$	
KTL	GITT	$2.53 \sim 3.32 \times 10^{-9}$	10.1021/acsaem.9b01526
NaFePO <sub>4</sub>	GITT	$1 \times 10^{-9} \sim 5 \times 10^{-8}$	10.1002/cssc.202000131
NaCoO <sub>2</sub>	GITT	$8.63 \times 10^{-17}$	10.1039/C2NR32758A
NaCoO <sub>2</sub>	EIS	$0.5 \sim 1.5 \times 10^{-10}$	10.1038/srep09006
Na <sub>3</sub> V <sub>2</sub> (PO <sub>4</sub> ) <sub>3</sub> /C	GITT	$10^{-12} \sim 10^{-14.5}$	10.1039/C5TA00765H

**Table S6.** Li-ion diffusion coefficient of representative imide-type electrodes in LIBs

Materials	Technique	Diffusion coefficient (cm <sup>2</sup> s <sup>-1</sup> )	Ref.
-----------	-----------	---	------

	EIS	$2.3 \times 10^{-14}$	10.1002/celc.202000118
 BTAQ	GITT	$2.18 \times 10^{-13}$ $\sim 2.23 \times 10^{-14}$	10.1039/c9ta05552e
	EIS	$2.1 \times 10^{-9}$	10.1002/chem.201703823

## Reference

S1. Frisch, M. J., Trucks, G. W., Schlegel, H. B., Scuseria, G. E., Robb, M. A., Cheeseman, J. R., Scalmani, G., Barone, V., Mennucci, B., Petersson, G. A., Nakatsuji, H., Caricato, M., Li, X., Hratchian, H. P., Izmaylov, A. F., Bloino, J., Zheng, G., Sonnenberg, J. L., Hada, M., Ehara, M., Toyota, K., Fukuda, R., Hasegawa, J., Ishida, M., Nakajima, T., Honda, Y., Kitao, O., Nakai, H., Vreven, T., Montgomery, J. A., Peralta, Jr. J. E., Ogliaro, F., Bearpark, M., Heyd, J. J., Brothers, E., Kudin, K. N., Staroverov, V. N., Keith, T., Kobayashi, R., Normand, J., Raghavachari, K., Rendell, A., Burant, J. C., Iyengar, S. S., Tomasi, J., Cossi, M., Rega, N., Millam, J. M., Klene, M., Knox, J. E., Cross, J. B., Bakken, V., Adamo, C., Jaramillo, J., Gomperts, R., Stratmann, R. E., Yazyev, O., Austin, A. J., Cammi, R., Pomelli, C., Ochterski, J. W., Martin, R. L., Morokuma, K., Zakrzewski, V. G., Voth, G. A., Salvador, P., Dannenberg, J. J., Dapprich, S., Daniels, A. D., Farkas, O., Foresman, J. B., Ortiz, J. V., Cioslowski, J., Fox, D. J. *Gaussian, Inc., Wallingford CT*, 2013.